Macrophage Cholesterol Homeostasis Underpins the role of Sertraline as an Adjunctive Agent in Tuberculosis Therapy.

Kanika Bisht [1,2], Riya Sahu [1,2], Nikita Bhor [1,2], Simran Jit [1,2], Jitendra Kumar [1], Mahima Madan[1,2], Deepthi Shankaran [1,2], Sherry Bhalla [1,2], Vivek Rao [1,2]*

1-CSIR- Institute of Genomics and Integrative Biology, Mathura Road, New Delhi-110025 India.

2- Academy of Scientific and Innovative Research (AcSIR), Ghaziabad, 201002, India

*Corresponding author: Tel: +91 11 29879229, E-mail: vivek.rao@igib.res.in.

Key words: *Mycobacterium tuberculosis*/ host-directed therapy/ antidepressant/ sertraline

Running Title: Cholesterol flux dictates bacterial control

Abstract:

An intricate relationship exists between metabolism and the macrophage response in controlling intracellular pathogens such as Mycobacterium tuberculosis (Mtb). Here, we identify a deterministic role for macrophage cholesterol metabolism in the efficacy of anti-tubercular therapy (ATT). We that sertraline (SRT), an FDA-approved antidepressant, capable of enhancing tuberculosis treatment, rewires the macrophage lipid metabolism to potentiate Mtb clearance. Treatment with SRT leads to lysosomal cholesterol accumulation thereby activating the cholesterol-sensing transcription factor SREBP2 and increasing biosynthetic cholesterol flux in macrophages. In addition, this buildup of cholesterol induces lysosomal membrane permeabilization (LMP), mitochondrial ROS production, and downstream NLRP3 inflammasome activation, contributing to enhanced macrophage-mediated bacterial killing. Our results thus highlight a previously underappreciated link between cholesterol homeostasis and inflammasome activation, which contributes to improved Mtb clearance in the presence of adjunctive sertraline therapy.

27 **Graphical abstract:**

28

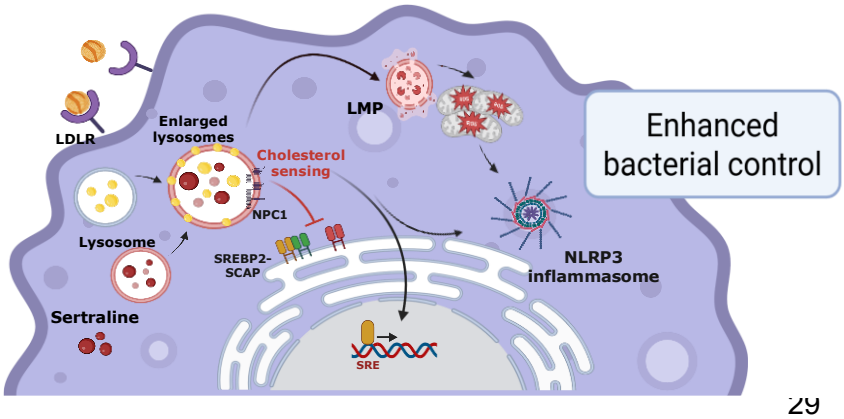

SRT induced lysosomal cholesterol accumulation results in enhanced bacterial control via inflammasome activation

29

30 **Introduction:**

31 Tuberculosis (TB), caused by *Mycobacterium tuberculosis* (Mtb), remains the leading cause of
32 death by a single infectious agent globally, outpacing all other bacterial and viral pathogens [1-3].
33 The multiple initiatives to curb the infection have not been successful enough to eradicate the
34 disease, instead have led to an increase in drug resistance in the population [4,5]. These limitations
35 have spurred an interest in therapeutic strategies designed to aid the host in controlling infection.
36 Such host-directed therapies (HDTs) have relied on harnessing the cellular physiological
37 pathways to enhance antimicrobial properties [6-8]. We have previously shown that sertraline (SRT),
38 a selective serotonin reuptake inhibitor (SSRI), can act as a potent adjunct to standard anti-TB
39 therapy (ATT), accelerating bacterial clearance, improving tissue resolution, and enhancing host
40 survival in preclinical infection models [9]. These properties are associated with the restriction of
41 type I IFN responses via the activation of the host inflammasome pathway, thus defining the
42 therapeutic potential of manipulating host immunity for infection control [10].
43 Recent findings strongly advocate for the influence of host sterol metabolism in regulating the
44 inflammatory capacity of innate immune cells [11-13]. More importantly, oxysterols have emerged as
45 promoters of the pro-inflammatory capacity of macrophages [14,15]. Recently, the ability of SREBP2,

46 the master regulator of cellular cholesterol metabolism, to directly activate the host cell
47 inflammasomes via the NLRP3 axis[16].
48 Here, we demonstrate that treatment with SRT leads to a significant increase in intracellular
49 cholesterol levels in Mtb-infected macrophages—an effect critical for enhanced bacterial control.
50 In light of these observations, we sought to investigate whether sertraline's adjunctive efficacy is
51 mechanistically linked to its influence on host cholesterol metabolism. By employing chemical
52 modulation and gene silencing, we demonstrate that the SRT-mediated cholesterol buildup
53 perturbs lysosomal integrity, thereby promoting mitochondrial reactive oxygen species (ROS)
54 production and thus cascading into the activation of the NLRP3 inflammasome. Taken together,
55 our findings provide a mechanistic link between cellular metabolic machinery, particularly
56 cholesterol metabolism, and antimicrobial efficacy, offering both conceptual and translational
57 insights into how metabolic reprogramming can be leveraged for augmenting host immunity as a
58 host-directed therapeutic strategy to improve TB treatment outcomes.

59 **Results:**

60 **Treatment with sertraline increases cellular cholesterol in macrophages**

61 In an attempt to decipher the underlying mechanism for sertraline- mediated increase of antibiotic
62 efficacy in Mtb infections, global expression profiles of Mtb-infected THP1 macrophages with a
63 combination of isoniazid (H) and rifampicin (R) with (SRT) were compared with HR-treated cells.
64 A total of 160 genes of cholesterol homeostasis were differentially upregulated on treatment with
65 HRS when compared to HR treatment (Figure 1A). Interestingly, cholesterol homeostasis
66 emerged as the only significantly enhanced metabolic pathway along with an increase in the
67 mTORC1 signaling complex in macrophages treated with HRS (Figure 1B). In fact, HRS-treated
68 macrophages displayed a significant increase in the expression of genes involved in cholesterol
69 biosynthesis (Figure 1C) and import, with the markedly lower expression of sterol export genes
70 (Figure 1D). A similar pattern was reflected in SRT or HRS-treated macrophages by qRT-PCR.
71 While infection or treatment with HR failed to alter expression of genes involved in cholesterol

72 metabolism, genes involved in biosynthesis and import were 3-5-fold higher upon treatment with

73 HRS or SRT at 24 h of infection (Figure 1E). This increment in gene expression reflected as an

74 SRT-dependent 1.2-1.5-fold increase in intracellular cholesterol (Figure 1F).

75

76

77

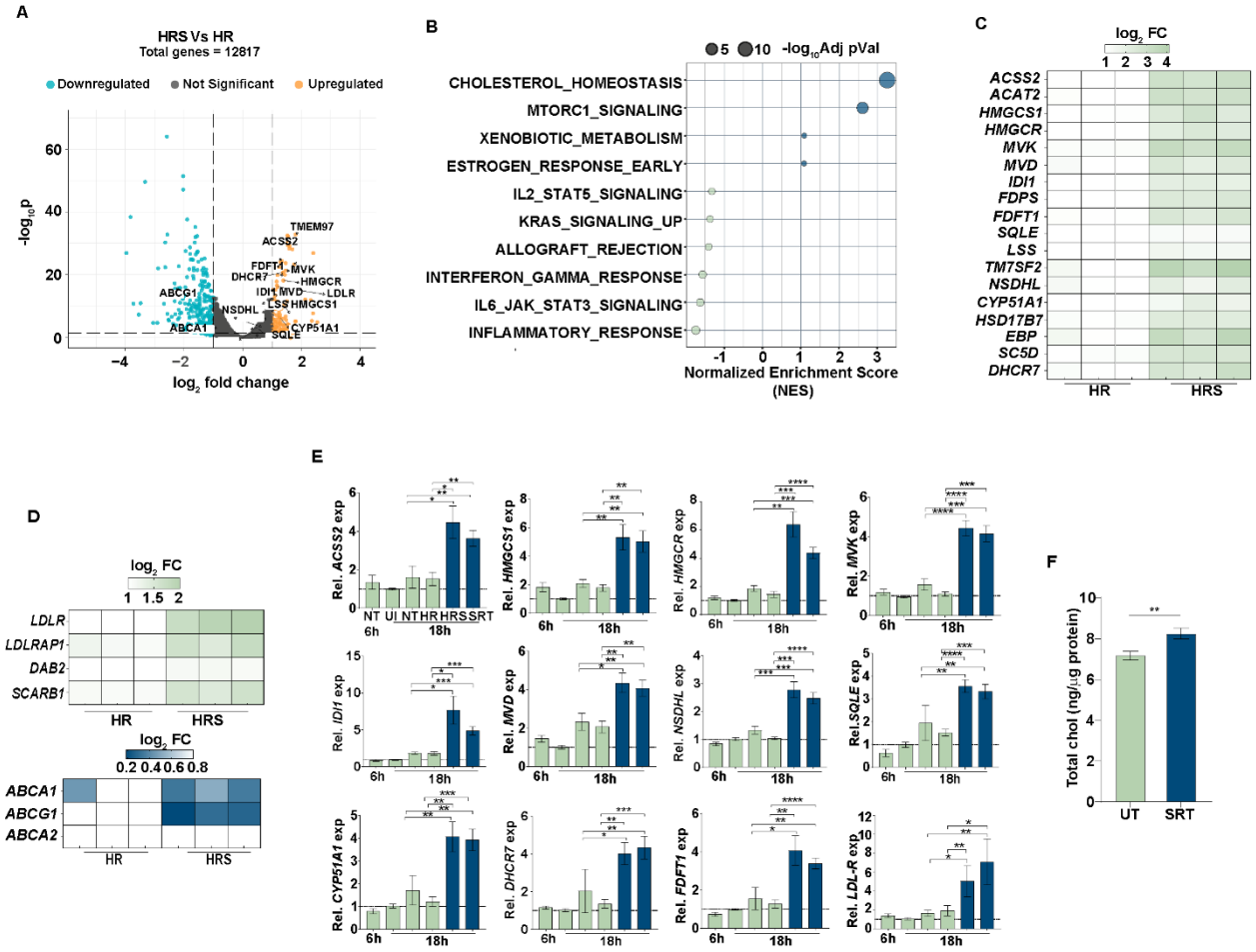

Figure 1

78

79 **Figure 1: Global transcriptomics of Mtb-infected macrophages following treatment with sertraline.**

80 A) A comparison of the differentially expressed genes in Mtb-infected macrophages following an 18 h

81 treatment with HR or HRS is shown as a volcano plot. Y- and X-axes denote the -$\log_{10}$ P values

82 and log_2 fold change, respectively. The upregulated genes with ≥ 2 fold change with p-value of ≤
83 0.01 are highlighted in orange, while the downregulated genes with ≤ -2 fold change with p-value
84 of ≤ 0.01 are in blue.
85 B) GSEA analysis of the top significantly enriched gene sets in HRS vs HR is represented as a bubble
86 plot. Gene sets that are significantly (P-value ≤ 0.05, 0.01) enriched (Blue) or downregulated
87 (green) are represented, with the X-axis denoting the normalized enrichment score.
88 C-E) Gene expression patterns in HR and HRS-treated macrophages: Expression of genes involved in
89 cholesterol biosynthesis (C) and cholesterol trafficking (D) in the RNA -seq data was validated by
90 gene specific qRTPCR (E). The relative expression of specific genes relative to *GAPDH* is
91 represented as fold change w.r.t uninfected control (UI) at 6h ± SEM of triplicate assays from 3
92 independent experiments (N=3).
93 F) Cholesterol levels in THP1 macrophages after treatment with sertraline (SRT) for 24 hours. Total
94 free cholesterol was normalized to the amount of protein and is represented as mean ± SEM for
95 triplicate assays of three independent experiments (N=3).
96 P values less than 0.05, 0.01, 0.005 are represented as *, ** and *** respectively.
97

98 **Increased intracellular cholesterol biosynthesis is critical for the beneficial effect of**
99 **sertraline on bacterial control**.

100 Given the increment in cellular cholesterol levels, we sought to modulate the cholesterol flux in
101 macrophages and analyze its effect on antibiotic efficacy. To enhance the cholesterol biosynthetic
102 flux without the addition of SRT, Mtb-infected macrophages were exogenously supplemented with
103 mevalonate [17], along with anti-TB drugs (HR). This resulted in a 2-3-fold improved bacterial control
104 by HR-treated macrophages in comparison to non-supplemented cells, comparable to the
105 addition of SRT to HR (Figure 2A). Supplementation did not affect the growth of bacteria in
106 macrophages without any antibiotic treatment hinting at the importance of sterol homeostasis
107 specifically in antibiotic mediated growth control. To restrict cholesterol biosynthesis, cells with 3-
108 4-fold lower levels of *HMGCR*, were developed by gene-specific silencing (Figure 2B), and the

109 effect of this reduced expression on Mtb control was evaluated. Contrary to our expectations,
110 silencing *HMGCR* did not alter the effect of SRT on antibiotic mediated bacterial control (Figure
111 2C). We reasoned that silencing of *HMGCR* could be countered by SRT mediated increase in
112 expression. Alternatively, we employed pharmacological inhibition of *HMGCR* by simvastatin.
113 Contrary to our expectations of diminishing antibiotic efficacy, addition of statins significantly
114 enhanced the control of Mtb control by antibiotics by 3-5-fold in comparison to the cells treated
115 with HR or HRS alone (Figure 2D). Further, the impact of cholesterol influx on the effect of SRT
116 was evaluated by modulating the import of sterol via the low-density lipoprotein receptor (LDL-r)
117 from the extracellular milieu with the use of lipoprotein -deficient serum (LPDS) with and without
118 LDL supplementation for treatment. While the use of LPDS did not affect Mtb growth control by
119 antibiotics alone or in combination with SRT (HR, HRS), replenishment with LDL in LPDS
120 significantly reversed the effect of SRT with a 3-fold increase in the bacterial numbers in HRS-
121 treated cells (Figure 2E).
122 Given the observation that statins, despite restricting serum cholesterol, actually enhance the
123 cellular cholesterol biosynthesis rate along with its import, with a significant reduction in
124 cholesterol export [18,19], we tested for the levels of total cellular cholesterol and gene expression
125 following treatment with statins. Treatment with simvastatin enhanced total cholesterol in cells as
126 well as induced the expression of the genes of the biosynthetic pathway (Figures- S1A, S1B).
127 This suggested that the increased flux of the pathway may be crucial in enhancing bacterial
128 control by SRT. A similar effect was also observed in macrophages grown in LPDS-containing

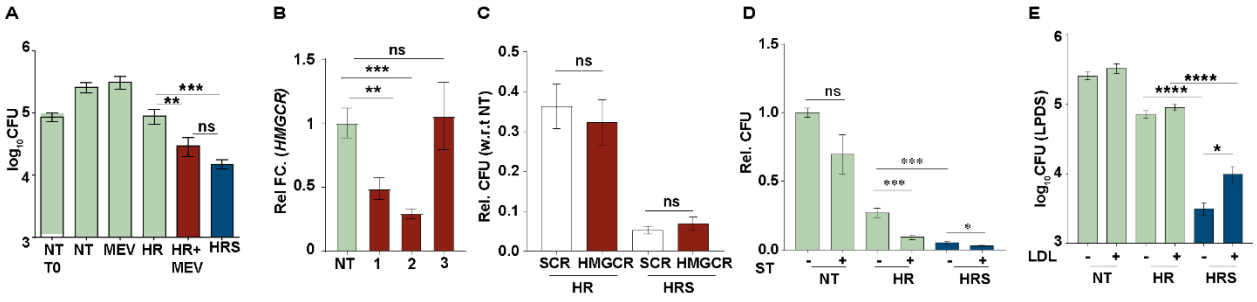

Figure 2

129 media, marked by a significant increase in cholesterol biosynthesis and total cellular cholesterol
130 levels comparable to cells grown in FBS, substantiating the importance of cholesterol biosynthesis
131 in SRT-dependent increment of bacterial control (Figures- S1C, S1D).
132
133
134 **Figure 2: Effect of modulating cholesterol homeostasis on sertraline efficacy.**
135 A) Growth of Mtb in macrophages supplemented with mevalonate (MEV) either alone or in
136 addition to HR after 3 days. HRS-treated cells were used as a control for positive growth
137 restriction.
138 B-C) Effect of HMGCR silencing on Mtb growth in macrophages. HMGCR expression levels
139 were evaluated by qRT PCR and is represented as mean fold change ± SEM w.r.t
140 scrambled (SCR) control (B) across three independent experiments (N=3). C) Bacterial
141 growth in HMGCR silenced macrophages treated with HR and HRS.
142 D-E) Growth of Mtb in HR or HRS treated macrophages that were treated with 10μM
143 simvastatin (ST) (D) or (E) cultured in cholesterol-depleted media (LPDS), for 3 days.
144 Bacterial numbers are represented as mean $\log_{10}$ CFU ± SEM from triplicate assays of three
145 or four independent experiments (N = 3 or 4). P values less than 0.05, 0.01, 0.005 are represented
146 as *, ** and *** respectively.
147
148 **Lysosomal cholesterol accumulation is crucial for Mtb control in macrophages**
149 Cholesterol levels in different subcellular locations are tightly regulated to maintain a steady state
150 in cells. To test the effect of increased cellular cholesterol on intracellular distribution,
151 macrophages were stained with the cholesterol specific dye- filipin and visualized by fluorescence
152 microscopy. While filipin staining was primarily concentrated on the membranes of untreated (UT)
153 cells with minimal staining within, treatment with SRT severely impacted intracellular sterol levels,
154 with cells displaying significantly higher intracellular staining in addition to the membrane (Figure

155 3A). To further identify the intracellular niche of the accumulated cholesterol, cells fed with NBD-
156 cholesterol ester were stained with the lysosomal stain-lysotracker. Again, while in the untreated
157 cells, minimal levels of cholesterol co-localized with lysosomes, the majority of the internalized
158 cholesterol in SRT treated cells was found to be accumulated in the lysosomal compartments,
159 indicating a pronounced accumulation of cholesterol in the lysosomal compartments with SRT
160 treatment (Figure 3B, C).
161 In order to understand if this increase in cholesterol biosynthesis was a generic property of SSRIs,
162 another widely used antidepressant, citalopram, was tested for its ability to control intracellular
163 bacterial growth. Surprisingly, the addition of citalopram to the frontline TB drugs-HR did not affect
164 bacterial control in macrophages, unlike the increased control of infection by HRS in comparison
165 to the antibiotics alone (Figure 3D). Remarkably, unlike SRT, citalopram failed to induce
166 cholesterol accumulation in the lysosomes or enhance the expression of cholesterol biosynthesis
167 in macrophages validating the importance of this mechanism in enhanced antibiotic control of Mtb
168 (Figure 3E, F).
169
170
171
172
173
174
175
176
177
178
179
180

181

182

183

184

185

186

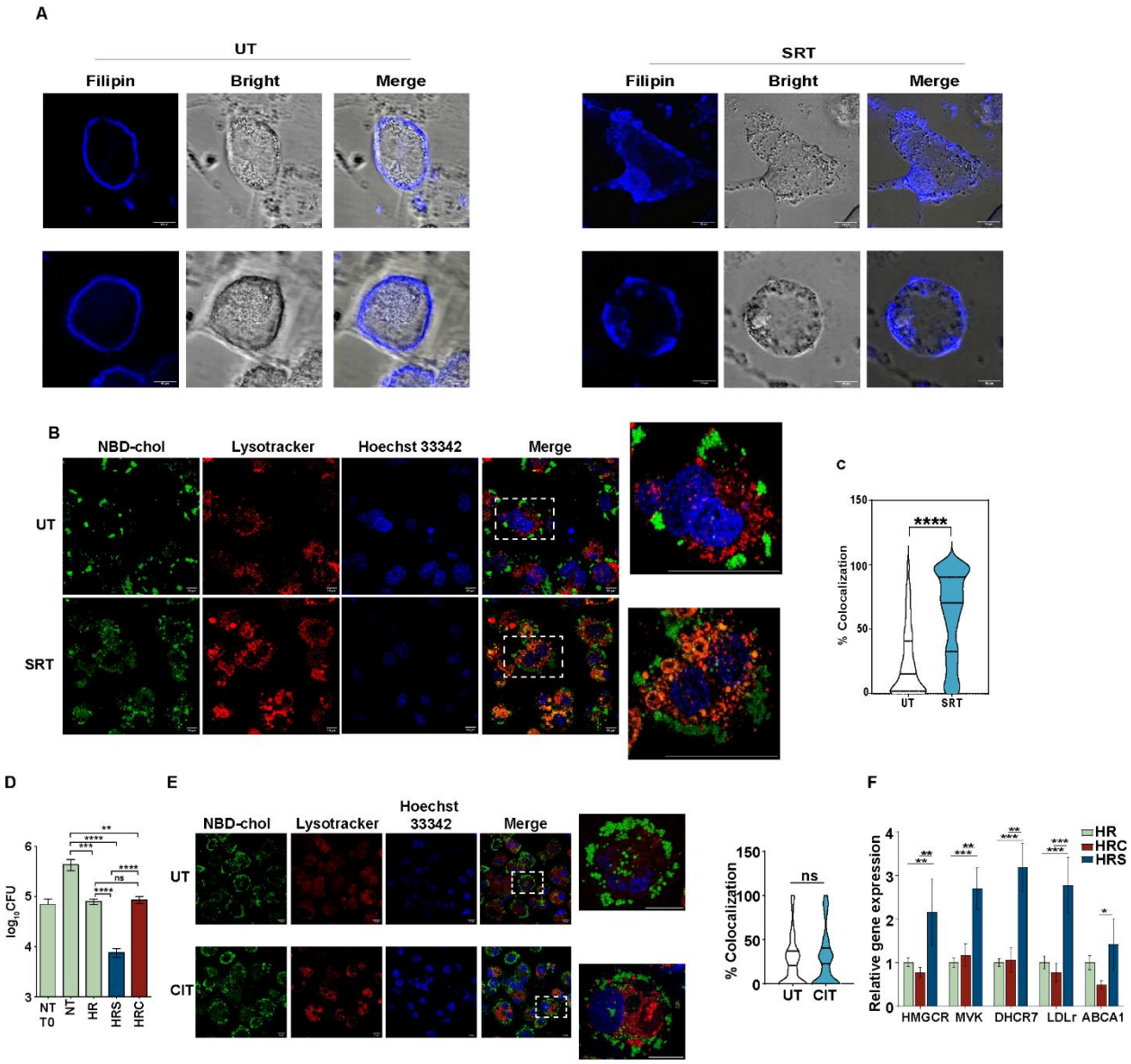

Figure 3

Figure 3: Sertraline treated macrophages accumulate lysosomal cholesterol.

A-B) Representative confocal images of THP1 macrophages after SRT treatment for 24 h stained with filipin (A) or fed with NBD-cholesterol and stained with lysotracker Red and Hoechst 33342 (B). The inset shows the zoom-in along the black lines. Scale bar = 10µm.

(C) The graph shows the percent colocalization of the NBD-cholesterol in the lysosomes from three independent experiments.

194 D) Intracellular bacterial growth was estimated in Mtb–infected THP1 macrophages left untreated (NT) or
195 treated with HR alone or in combination with 20 μM citalopram (CIT) for 3 days. The data are represented
196 as mean Log_{10} values ± SEM from triplicate assays of four independent experiments (N = 4).
197 E) Representative confocal images of THP1 macrophages treated with citalopram along with NBD-
198 cholesterol for 24 hours and stained with lysotracker Red, and the colocalization percentage is calculated
199 using ImageJ. Scale bar = 10μm.
200 F) Gene expression levels in macrophages infected with Mtb, followed by treatment with HR alone or with
201 citalopram. The relative expression of the specific gene, relative to GAPDH, is represented as fold change
202 with respect to HR ± SEM of triplicate assays from three independent experiments (N=3).
203 P values less than 0.05, 0.01, 0.005 are represented as *, ** and *** respectively.
204
205 **Sertraline enhances SREBP2 activation in macrophages**:
206 The feedback activation of SREBP2 (cholesterol biosynthetic machinery) in response to the
207 absence of cholesterol sensing in the ER on account of lysosomal sequestration is well
208 documented [20,21]. To assess whether SRT activates the signaling cascade, levels of mature
209 SREBP2 (mSREBP2) were measured in macrophages following SRT treatment. Indeed,
210 commensurate with the significant induction of the SREBF2 gene in HRS-treated macrophages,
211 in both the global transcriptomic data and with qRT-PCR analysis, macrophages treated with SRT
212 harbored ~2-fold higher levels of the cleaved, active form of SREBP2 (mSREBP2) by 24h
213 compared to the untreated cells (Figure 4A-D). The relatively unchanged levels of mSREBP2 in
214 both untreated and citalopram treated cells, lends further support to the importance of this
215 signaling axis in the antibiotic potentiating effect of SRT (Figure 4 E, F).
216

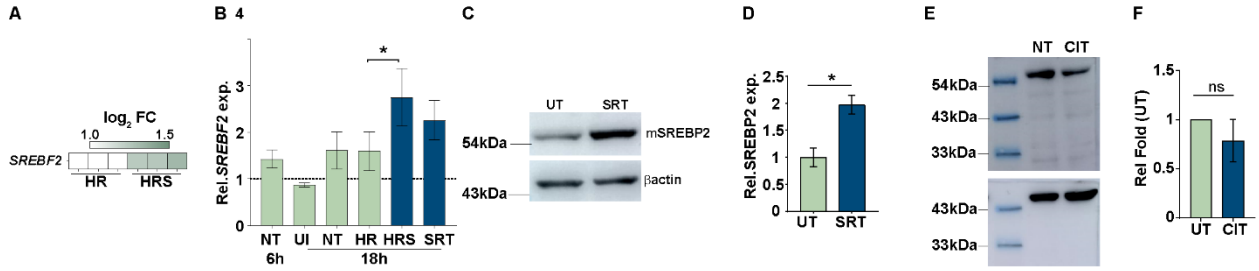

Figure 4

Figure 4: Sertraline enhances SREBP2 activation in macrophages.

A -B) Expression levels of *SREB*F2 in the global transcriptomic analysis dataset (A) or quantified by qRT-PCR (B) in Mtb-infected macrophages left untreated (NT) or treated with HR, HRS, or SRT for 18h. The relative expression of specific genes relative to *GAPDH* is represented as fold change ± SEM of triplicate assays of three independent experiments (N=3).

C-F) The levels of SREBP2 in protein extracts of macrophages left untreated, treated with SRT (C) or 20μM of citalopram (E) for 24 hours were checked by immunoblotting with specific antibodies for SREBP2 and β-actin and quantified by densitometry (D, F). The reactivity for SREBF2 in cells relative to β-actin was quantified in three independent experiments (N=3) and is represented as mean ± SEM.

P values less than 0.05, 0.01 and 0.005 are represented as *, ** and *** respectively.

SREBP2 activation is regulated by multiple feedback mechanisms; typically, cholesterol and oxysterols have been shown to downregulate this process by modulating the SCAP-SREBP2 egress to the Golgi [22]. To test the importance of SREBP2 activation on Mtb control, macrophages were treated with cholesterol exogenously to inhibit SREBP2 processing and tested for their ability to control Mtb growth in the presence of HR or HRS. Addition of cholesterol significantly inhibited SREBP2 activation (2-fold) (Figure 5A, Figure S1E) and resulted in a significant reversal of the effect of SRT on antibiotic potentiation (Figure 5B). Interestingly, even in the HR treated cells, the addition of cholesterol restricted the ability of HR to control bacterial growth with ~2-3-fold higher bacterial numbers (Figure 5B). Further, the inhibition of SREBP2 activation with a specific S2P

238 protease inhibitor- 1,10-phenanthroline, resulted in a significant but partial reversal of bacterial
239 control by SRT (3-4-fold higher bacterial numbers than HRS alone) (Figure 5C). To further test
240 the relevance of SREBP2 processing, macrophages deficient in the SREBP2 cleavage activation
241 protein (SCAP) were tested for their ability to restrict Mtb growth. As expected, THP1 lines with
242 >50% silencing of *SCAP* with specific shRNAs displayed significantly lower levels of SREBP2
243 activation in comparison to the cells treated with scrambled shRNAs (SCR) (Figure 5D-F).
244 Consistent with the inhibition of S2P, silencing of SCAP reduced the effectiveness of SRT on Mtb
245 control without affecting the uptake of bacteria (Figure 5G). As observed in Figure 5H, SCAP-
246 silenced macrophages harbored significantly higher bacterial numbers (3-4- fold) than the control
247 cells. Even in the untreated cells, loss of SCAP severely impaired the ability to control Mtb with
248 nearly 3-fold higher CFU in the SCAP-deficient cells than in the control (Inset, Figure 5H),
249 corroborating the requirement of SREBP2 activation in Mtb control by macrophages.

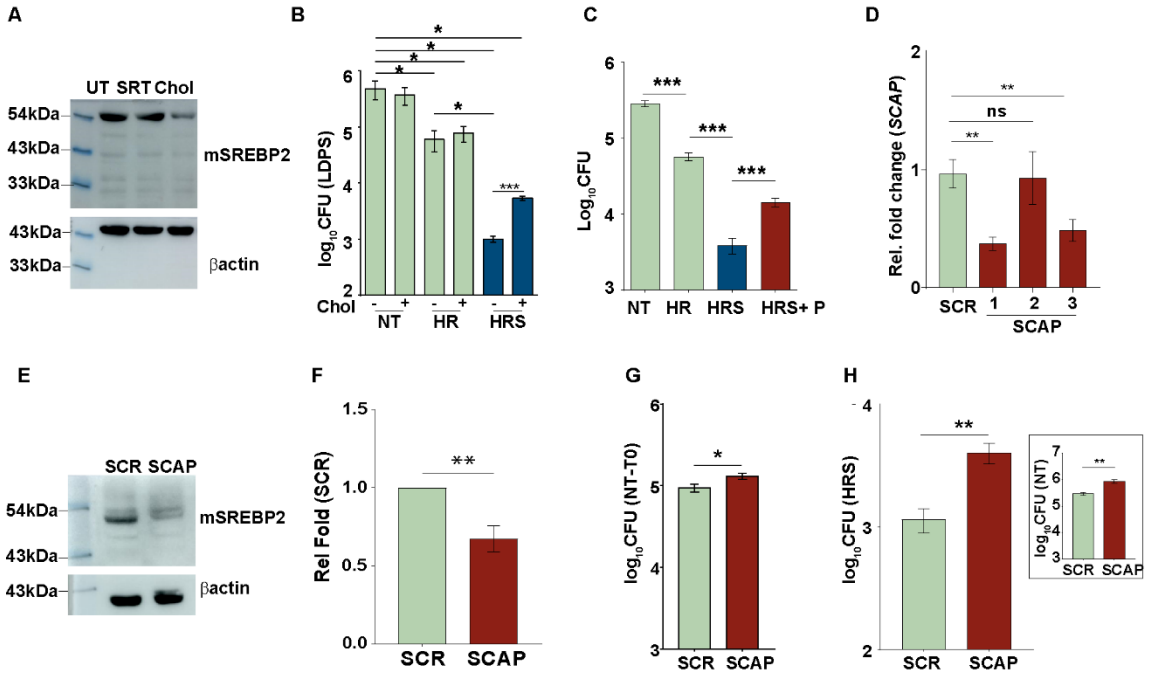

Figure 5

250

251

252

253 **Figure 5: Role of SREBP2 activation in restricting intracellular bacterial growth.**

254 A) The levels of SREBP2 in cell extracts of macrophages treated with 20µg/ml of cholesterol for 24 h
255 were analysed by immunoblotting. The levels of β-actin were used as the control values for the
256 comparison.

257 B-C) The intracellular bacterial growth was estimated in Mtb-infected macrophages that were either
258 untreated or treated with (B) cholesterol or (C)- 0.5 mM of 1,10-phenanthroline (P) for 1 hour. This
259 was followed by treatment with HR and HRS alone, in combination with cholesterol, which was
260 replenished every 24 hours in the LPDS media, or with 1,10-phenanthroline. The data is
261 represented as mean $\log_{10}$ values ± SEM from triplicate assays of four independent experiments
262 (N = 4).

263 (D) Evaluation of gene expression levels in *SCAP* silenced macrophages. The relative expression of the
264 *SCAP* is represented as fold change ± SEM w.r.t. scrambled control in triplicate assays from three
265 independent experiments (N=3).

266 (E) Estimation of activation of SREBP2 in protein extracts of *SCAP* silenced cells by immunoblotting
267 with specific antibodies for SREBP2 and β-actin.

268 (F) Densitometric quantification of the reactivity for SREBP2 in cells relative to β-actin of six independent
269 experiments (N=6) is represented as mean ± SEM.

270 (G) Bacterial uptake in *SCAP* silenced cells compared to scrambled control after 6 hours of incubation
271 with Mtb at MOI 5.

272 (H) Intracellular growth of Mtb is depicted in untreated (NT) (inset) or HRS-treated *SCAP* silenced cells.
273 The data are represented as mean $\log_{10}$ values ± SEM from triplicate assays of three independent
274 experiments (N = 3).

275 **SRT phenocopies the effects of NPC1 inhibition in cells**

276 A similar phenotype of organellar sterol accumulation, specifically in the endosomal-lysosomal
277 compartments, is a characteristic feature of NPC1 mutation/ deficiency in the human population
278 [23,24]. This phenotype can be recapitulated in cells by the addition of an NPC1 inhibitor- U18666A,
279 inducing pronounced accumulation of cholesterol in lysosomal compartments. To verify the
280 importance of increased SREBP2 processing in Mtb control, the effect of antibiotics was tested in

281 cells treated with U18666A. As expected, U18666A induced significant accumulation of NBD-
282 cholesterol in THP1 macrophages, with the majority of the lipid co-localized with the lysosomes
283 (Figure 6A). Consistent with this accumulation, U18666A-treated macrophages induced
284 significantly higher levels of SREBP2 activation than untreated cells and enhanced the expression
285 of the cholesterol biosynthetic machinery (Figure 6B, Figure S1F). This effect was also reflected
286 in the 3-4-fold better control of Mtb in macrophages treated with U18666A and the frontline TB
287 drugs -HR by day 3 of infection (Figure 6C), emphasizing the relevance of lysosomal cholesterol
288 loading in bacterial control. To simulate conditions of enhanced cholesterol biosynthesis via
289 increased SREBP2 activation, we resorted to silencing INSIG1, the inhibitor of SCAP-SREBP2
290 translocation for processing and activation at the Golgi and observed a significant (>60%)
291 decrease in the levels of INSIG1 expression (Figure 6D). However, we did not observe any
292 detectable change in the levels of SREBP2 activation in these macrophages (Figure 6E, Figure
293 S1G). As an alternative, macrophages were treated with brefeldin A (BFA) to facilitate constitutive
294 proteolysis and activation of SREBP2 due to the collapse of the ER- Golgi network [25]. In sync with
295 our expectations, the addition of BFA significantly increased the expression of active SREBP2 in
296 macrophages (2-fold- Figure S1H) that reflected as a 3-4-fold decrease in bacterial numbers in
297 HR treated cells, further emphasizing the importance of SRT mediated increase in SREBP2
298 activation in the ability of macrophages to restrict bacteria (Figure 6F, G).

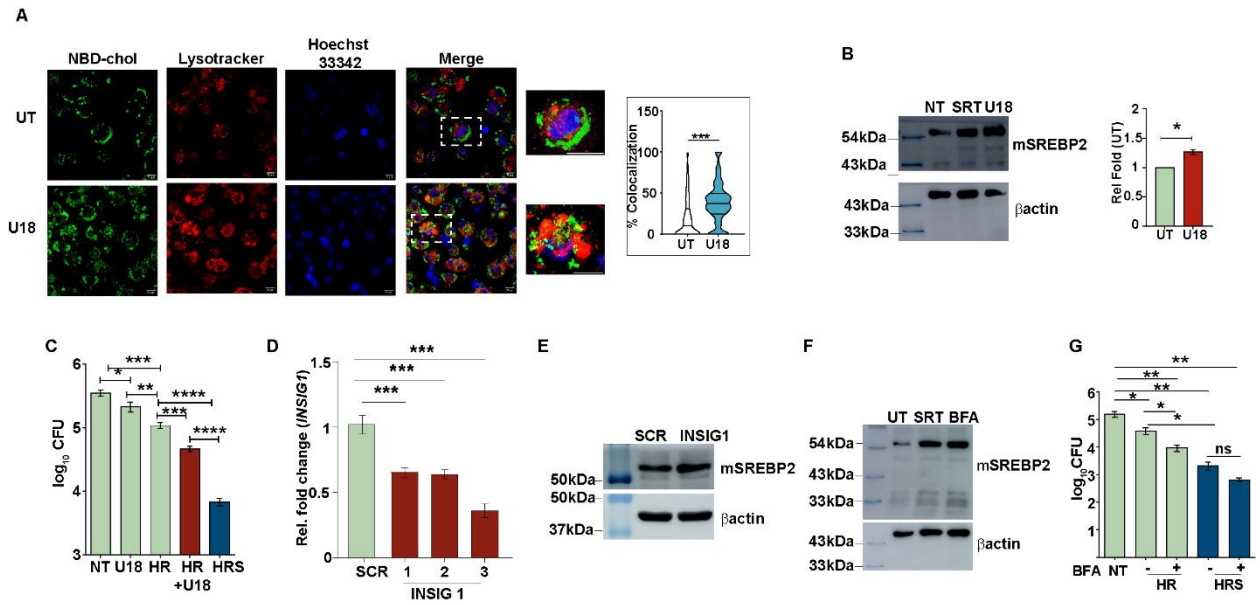

Figure 6

Figure 6: SRT treatment phenocopies NPC1 deficiency.

A) The localization of cholesterol was analysed in cells treated with 2.5 µg/ml of the NPC1 inhibitor-U18666A (U18). The extent of colocalization of NBD-cholesterol and lysosomes (lysotracker) in macrophages was quantified and is expressed as percent co-localization from three independent experiments (N=3) (inset).

B) The extent of SREBP2 activation was evaluated in macrophages left untreated or treated with U18666A by immunoblotting and densitometric analysis of the lysates. Levels of β- actin expression was used as the control. The relative levels of mSREBP2 in SRT treated cells (w.r.t. untreated) is represented as relative mean expression ± SEM from six independent experiments is shown in the box (N=6).

C) Growth of Mtb in macrophages that were left untreated or treated with HR alone or in combination with U18666A and HRS for 3 days. The CFU numbers are represented as mean $\log_{10}$ values ± SEM from triplicate assays of four independent experiments (N = 4).

D) Expression of *INSIG1* gene was quantified by qRTPCR. *GAPDH* expression values were used as controls for normalization. The relative expression in the *INSIG1* silenced cells was compared with

315 the scrambled control and is represented as Rel. fold change mean ± SEM of triplicate assays
316 from three independent experiments (N=3).
317 E-F) The levels of mature SREBP2 or β- actin were analyzed by specific immunoblotting of the lysates
318 from *INSIG1* -silenced macrophages and control cells (E) or in cells left untreated or treated with
319 3μg/ml BFA (F).
320 G) Growth of Mtb in macrophages left untreated or treated with HR, HRS alone or in combination
321 with brefeldin A (BFA) for 3 days. The CFU numbers are represented as mean $\log_{10}$ values ± SEM
322 from triplicate assays of three independent experiments (N = 3).
323 P values less than 0.05, 0.01 and 0.005 are represented as *, ** and *** respectively.

324 **Loss of lysosomal integrity couples SRT mediated cholesterol accumulation with**
325 **activation of inflammasomes**

326 Accumulation of cholesterol in lysosomes has been associated with a significant damage to the
327 lysosomal membrane, resulting in the formation of pores, a process called lysosomal membrane
328 permeabilization (LMP) [26,27]. This loss of membrane integrity is rapidly repaired by the recruitment
329 of the ESCRT complex via the lectin-galectin 3 [28]. Treatment with SRT significantly induced the
330 expression of *LGALS3* in Mtb infected macrophages (Figure 7A-B). To check if SRT compromised
331 the membrane integrity of lysosomes, cells expressing GFP tagged galectin 3 were treated with
332 SRT. As observed in Figure 7C, galectin3 was distributed uniformly in the untreated cells, in
333 contrast to the punctate signal in the cells treated with LLOme, a dipeptide documented to induce
334 lysosomal damage [29]. Interestingly, SRT- treated cells also displayed punctate signals unlike the
335 treatment with citalopram (Figure 7D), suggestive of extensive lysosomal damage. A close
336 connect between the host lysosomal cholesterol levels and mitochondrial function has been
337 established [30-32]. Accumulation of cholesterol in the lysosomes has been associated with altered
338 mitochondrial physiology, exacerbated ROS production, and disorders [33-36]. Given our previous
339 observation for an important role for inflammasome activation by SRT [9] via the induction of
340 mitochondrial ROS [10] and an elegant study by Guo et.al, 2018 establishing a direct link between

341 the activation of SREBP2 and inflammasome induction [37], the role of cholesterol accumulation by
342 SRT as a putative cause of inflammasome activation was evaluated in Mtb infections. In line with
343 our previous studies, while SRT induced significant ROS, citalopram failed to activate
344 mitochondrial ROS in macrophages (Figure 7E-G). A direct link between the host cell cholesterol
345 accumulation, increased SREBP2 activation, and inflammasome activity was probed in cells by
346 estimating the levels of IL1β secretion in the different macrophages. Inhibition of SRT mediated
347 SREBP2 activation in SCAP deficient cells reduced the secreted IL1β levels (Figure 7H). This
348 study thus firmly establishes the importance of the cationic amphiphilic property of SRT in
349 augmenting bacterial control, thereby providing a novel target for the future development of host-
350 directed therapy against infections.
351

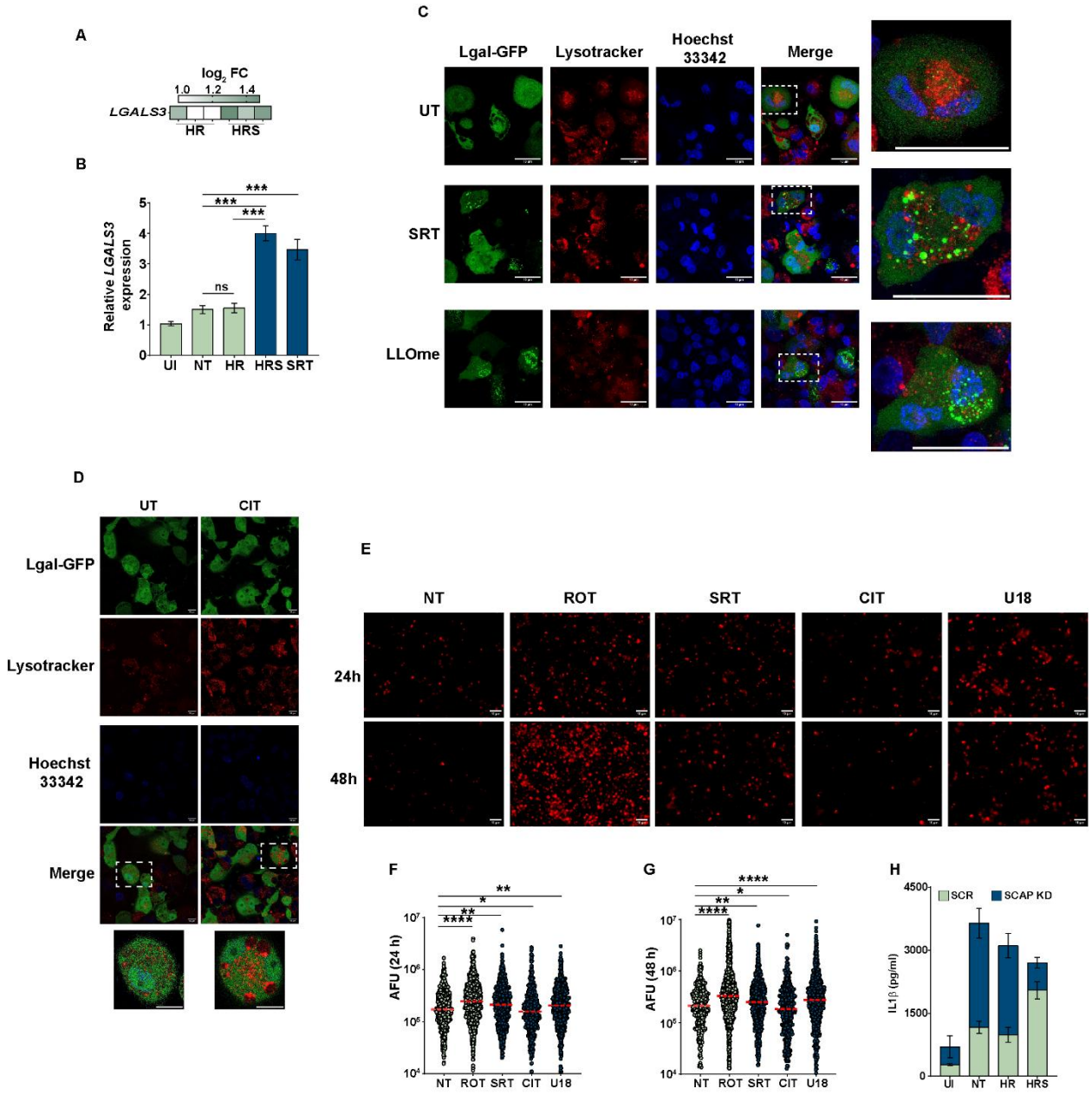

Figure 7

Figure 7: SRT-induced lysosomal cholesterol accumulation induces macrophage inflammasome

(A-B) Gene expression of *LGALS3* (A) in the transcriptomics data and quantified by qRT-PCR (B) in the Mtb-infected macrophages after 18 hours of treatment with HR, HRS, and SRT. The relative expression of

358 specific genes relative to *GAPDH* is represented as fold change ± SEM of triplicate assays of three
359 independent experiments (N=3).
360 (C) Representative images of macrophages overexpressing GFP-tagged galectin 3 protein treated with
361 SRT for 24 hours or LLOme for 15 min and stained with lysotracker Red. Boxes indicate insets, magnified
362 on the right. Scale bar = 10μm.
363 (D) Images after citalopram treatment for 24h in GFP-tagged galectin3 overexpressing macrophages. Inset
364 represents the zoom-in. Scale bar = 10μm.
365 (E-G) Representative images showing mitoSox staining after treatment with sertraline (SRT), citalopram
366 (CIT), U18666A (U18) and rotenone (ROT) as the positive control for mitochondrial ROS induction. The
367 extent of ROS was quantified after 24 h (F) and 48 h (G) of treatment and is represented as arbitrary
368 fluorescence units (AFU) from ~ 800 cells of three independent experiments (N=3).
369 (H) IL-1β levels in the supernatants of Mtb-infected SCR and *SCAP*- silenced cells following treatment with
370 HR or HRS, compared to the untreated group.
371 P values less than 0.05, 0.01 and 0.005 are represented as *, ** and *** respectively.
372 **Discussion:**
373 Infection control by innate immune cells is a complex process with the involvement of multiple
374 modalities, intertwining metabolic and inflammatory response pathways to ensure pathogen
375 removal [38,39]. The complexity only increases with the pathogen adept at modifying signaling
376 cascades and occupying intracellular niches that are designed for infection control [40,41]. The
377 incidence of TB, particularly, has been strongly associated with severe malnutrition[40,41].
378 Epidemiological data suggest a strong inverse correlation between serum cholesterol levels and
379 TB incidence and mortality, with TB patients displaying severe hypocholesterolemia [42-44]. In fact,
380 the enhanced levels of sputum sterilization in a small set of pulmonary TB patients on a
381 cholesterol-rich diet only highlight the importance of improving sterol levels for improved treatment
382 outcomes[45]. Recent studies have also implicated a significant role of cholesterol and its
383 derivatives in dictating macrophage response dynamics [46,47]. In line with these observations, we

384 identified an important role for the host cell cholesterol metabolic flux in the antibiotic mediated
385 potentiation of Mtb control by SRT.
386 In this context, we demonstrate that SRT treatment enhances macrophage cholesterol
387 biosynthetic and import programs through robust activation of the SREBP2 pathway, leading to
388 elevated intracellular cholesterol. We thus reasoned that altering cholesterol flux in macrophages
389 would modulate the effects of sertraline. To our surprise, sertraline activity remained unaltered
390 even in conditions of restricted biosynthesis (via statins [48] or HMGCR silencing) or import
391 (lipoprotein-deficient media). Contrary to our expectations, SRT treatment in LPDS or in the
392 presence of statins, as reported earlier [18], increased the expression of the cholesterol biosynthetic
393 genes in macrophages, resulting in enhanced effect of antibiotics in controlling infection, implying
394 the compensatory activation of alternative pathways to maintain homeostasis of cholesterol in
395 cells. The induction of HMGCR following SRT treatment in macrophages further hampered our
396 efforts to restrict biosynthetic flux by silencing HMGCR, bacterial control by SRT was unaltered in
397 these macrophages in comparison to the SCR cells.
398 Notably, SREBP2 axis emerged as a critical focal point connecting cholesterol metabolism and
399 infection control in macrophages. In concordance with recent studies that suggest a dominant
400 role for statins, we also observed significant activation of SREBP2 with SRT treatment in
401 macrophages, necessary for increased bacterial control [49-51]. However, both genetic perturbation
402 (silencing SCAP) and pharmacological activation (BFA), but not silencing of *INSIG1* (induced by
403 SRT in macrophages), confirmed the essential role of this pathway in SRT-mediated Mtb
404 restriction.
405 Our data relates the altered cholesterol trafficking and storage as vital mediators of SRT function.
406 Recently, TMEM97, a cholesterol-responsive NPC1-binding protein, has been implicated in
407 cholesterol trafficking between lysosomes and ER; RNA-interference mediated restraint of
408 TMEM97 reduces lysosomal lipid storage and restores cholesterol levels in the ER in cell models
409 of NPC1 [52]. SRT-treated macrophages with increased expression of TMEM97 (Data not shown)

410 resonate phenotypes with Niemann-Pick type C disease, with cholesterol-laden lysosomes and
411 disrupted ER-lysosome crosstalk. Along similar lines, treatment with the potent NPC1 inhibitor
412 U18666A induced significant dysregulation of cholesterol trafficking from lysosomes to the
413 endoplasmic reticulum (ER). Consistent with this, cells treated with either SRT or U18666A—but
414 not with citalopram—exhibited markedly enlarged lysosomes, indicative of cholesterol
415 accumulation.
416 This lysosomal sequestration appears to be a key trigger for downstream immune responses.
417 Oxysterols, particularly 25-hydroxy cholesterol (25HC), a dominant negative regulator of
418 cholesterol biosynthesis [53]acts as a dampener of inflammation, preventing the overstimulation of
419 macrophages by downregulating cholesterol biosynthesis and SREBP2 processing, in addition to
420 activating the esterification of excess free cholesterol [54,55]. 25HC is documented to protect
421 macrophages against mitochondria induced NLRP3 inflammasome activation with ch25h$^{-/-}$
422 macrophages the gene encoding for 25HC, elaborating significantly high levels of IL1β in in
423 response to LPS stimulation [56,57]. Mitochondrial ROS, SCAP-SREBP2 and the *FASN* effectively
424 mediate NLRP3-mediated inflammasome activation in cells [37,58,59]. Reduced expression of *CH25H*
425 (2-fold) and upregulation of *FASN* (~ 3-fold) suggest a coordinated suppression of anti-
426 inflammatory oxysterol signaling and a shift towards an activated inflammatory state. This
427 metabolic-inflammatory axis distinguishes SRT from related SSRIs such as citalopram, which
428 lacks these effects. In contrast, citalopram had an insignificant effect on these processes, thereby
429 validating the critical role of host cell cholesterol metabolism in macrophage-mediated control of
430 Mtb. These findings further support a model in which host cell cholesterol metabolism plays a
431 critical role in regulating mitochondrial stress and inflammasome activation, thereby contributing
432 to macrophage-mediated control of Mtb.
433 Further, the observed increase in assembly of galectin 3 close to the lysosomes in SRT-treated
434 macrophages advocates for extensive lysosomal membrane permeabilization (LMP) as a result
435 of lysosomal cholesterol accumulation, which is a property with lysosomotrophic molecules like

436 cationic amphiphilic drugs (CADs) [60]. While similar effects were observed with SRT and U18666A,
437 with strong experimental evidence as a CAD, citalopram a less well-documented cationic
438 amphiphile, failed to induce cholesterol accumulation and resultant LMP.
439 Our findings advance a previously understudied axis of reprogramming macrophage cholesterol
440 metabolism and the consequent induction of a lysosomal stress response that enhances
441 inflammasome activation and bacterial clearance (as seen with SRT). These findings emphasize
442 the significance of evaluating host metabolic programs for the design of future adjunct therapies
443 for infection control, specifically in the population cohorts with malnutrition and dyslipidemia.
444 Taken together, our work integrates lipid metabolism and innate immune signaling and places
445 host cholesterol metabolism as a crucial determinant of TB pathogenesis and treatment outcome.

446 **Author contribution**

447 KB and VR were instrumental in the design of the work. KB, RS, NB, JK, MM and DS were
448 involved in the conduct of the work. SJ and SB were involved in the analysis of the transcriptome
449 high throughput data. None of the authors have any conflict of interest.

450 **Acknowledgements**

451 The authors thank CSIR (VR- MLP2106) for supporting the study. CSIR-STS0016 is
452 acknowledged for continuous maintenance of BSL3 and ABSL2 facilities. CSIR- BSC0403 is duly
453 acknowledge for the microscopy facility. The student fellowships from CSIR- India (KB) are
454 acknowledged. Biorender.com is duly acknowledged for the graphical abstract preparation. The
455 authors thank Ms. Garima Maurya and Mr. Lakshay Kumar for proof reading and suggestion on
456 improving the manuscript. The authors thank Dr. Micheal Glickman for the LPDS media.

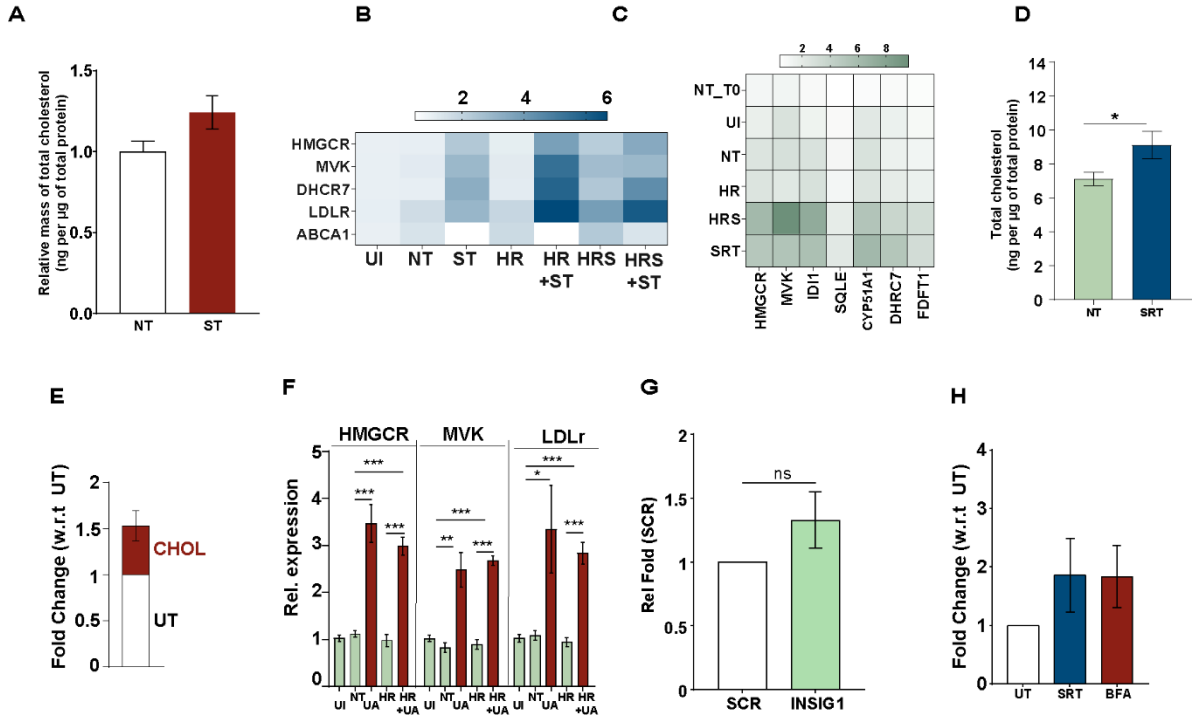

Figure S1

A-D) Effect of simvastatin (A, B) or LPDS supplemented media (C, D) on macrophage cholesterol levels were analysed at the metabolite (A, D) and expression of genes for biosynthesis (B, C) after 24h of treatment. Values represent the relative mean concentrations of statin treated cells as compared to untreated cells from triplicate assays of three independent experiments (N=3). The relative expression of specific genes relative to GAPDH is represented as fold change ± SEM of triplicate assays of three independent experiments (N=3).

E) The extent of SREBP2 activation was evaluated in macrophages left untreated or treated with cholesterol for 24h by immunoblotting and densitometric analysis of the lysates. Levels of β- actin expression was used as the control. The relative levels of mSREBP2 in cholesterol treated cells (w.r.t. untreated) is represented as relative mean expression ± SEM from three independent experiments is shown in the box (N=3).

F) Expression of genes for cholesterol biosynthesis were quantified by qRT-PCR in the Mtb-infected macrophages left untreated or after 18 hours of treatment with HR with and without U8666A (UA). The

472 relative expression of specific genes relative to GAPDH is represented as fold change + SEM of
473 triplicate assays of three independent experiments (N=3).
474 G, H) The extent of SREBP2 activation was evaluated in Wt or *INSIG1* silenced macrophages (G) or
475 left untreated or treated with 3μg/ml brefeldin A (H) for 24h by immunoblotting and densitometric
476 analysis of the lysates. Levels of β- actin expression was used as the control. The relative levels of
477 mSREBP2 in cholesterol treated cells (w.r.t. untreated) is represented as relative mean expression ±
478 SEM from three independent experiments is shown in the box (N=3).
479

480 **STAR METHODS**

481 **KEY RESOURCE TABLE**

REAGENT or RESOURCE	SOURCE	IDENTIFIER
Antibodies		
Rabbit polyclonal anti- SREBP2	Invitrogen	Cat# PA1-338
Mouse monoclonal anti-β-actin	Santa Cruz biotechnology	Cat#sc-47778
Bacterial and virus strains		
Mtb Erdman strain	Animal passaged strain EF2	NA
Chemicals, peptides, and recombinant proteins		
HiGlutaXL-RPMI-1640	Himedia	Cat# AL060G
DMEM high glucose	Himedia	Cat# AL007A
Sodium pyruvate	Himedia	Cat# TCL015
Fetal bovine serum	Himedia	Cat# RM9955
Fetal bovine serum lipid depleted	Biowest	Cat# S180L

Phorbol 12-Mysristate 13-acetate(PMA)	SIGMA	Cat# P8139
Ethambutol dihydrochloride	SIGMA	Cat# E4630
Isoniazid	SIGMA	Cat# I3377
Rifampicin	Himedia	Cat# CMS1889
Pyrazinamide carboxamide	SIGMA	Cat# P7136
Sertraline	SIGMA	Cat# S6319
Citalopram hydrobromide	SIGMA	Cat#C7861
U18666A	SIGMA	Cat#U3633
Mevalonic acid lithium salt	SIGMA	Cat#50838
Simvastatin	SIGMA	Cat#S6196
Cholesterol	SIGMA	Cat#C3045
Lipoprotein, low density, from human plasma	SIGMA	Cat#L7914
1,10 Phenanthroline	SIGMA	Cat#131377
Brefeldin A	Invitrogen	Cat#00450651
NBD- cholesterol	Avanti	Cat# 810250P
LysoTracker Red DND-99	Invitrogen	Cat#L7528
Hoechst 33342	Gift	NA
Filipin III readymade solution	SIGMA	Cat# SAE0087
Rotenone	SIGMA	Cat# R8875
MitoSox dye	Thermo Fisher Scientific	Cat# M36008
Lipopolysacchride (LPS)	InvivoGen	Cat# tlrl-smlps

Nigericin	Cayman Chemical	Cat# 28643-80-3
Lipofectamine LTX reagent with Plus reagent	Thermo Fisher Scientific	Cat# 15338100
Puromycin dihydrochloride	Himedia	Cat# TC198
Cholroform EMPARTA grade	Merck	Cat# 1.07024.2500
Methanol HPLC grade	Merck	Cat# 60600725001730
16% methanol free formaldehyde	Thermo Fisher Scientific	Cat# 28908
Critical commercial assays		
BCA protein estimation kit	GBiosciences	Cat#786-571
Total cholesterol	Abcam	Cat#ab282928
Human IL-1β ELISA kit	BD	Cat#557953
ECL Western Blotting Substrate	Promega	Cat#W1015
Deposited data		
RNA sequencing info		
Experimental models: Cell lines		
THP1 cells	ECACC	
THP1 Dual cells		
Lenti-X 293T		
THP1/NT shRNA	This study	N/A
THP1/SCAP shRNA#1	This study	N/A
THP1/SCAP shRNA#2	This study	N/A

THP1/SCAP shRNA#3	This study	N/A
THP1/Insig1 shRNA#1	This study	N/A
THP1/Insig1 shRNA#2	This study	N/A
THP1/Insig1 shRNA#3	This study	N/A
THP1/HMGCR shRNA#1	This study	N/A
THP1/HMGCR shRNA#2	This study	N/A
THP1/HMGCR shRNA#3	This study	N/A
THP1/GFP-tagged Gal3 overexpression	This study	N/A
Oligonucleotides		
Human *GAPDH* primer forward: 5'-GAAGGTGAAGGTCGGAGTC-3'	This study	N/A
Human *GAPDH* primer reverse: 5'-GAAGATGGTGATGGGATTTC-3'	This study	N/A
Human *ACSS2* primer forward: 5'-CATCAGCTTCTGGTCCAAGTG-3'	This study	N/A
Human *ACSS2* primer reverse: 5'-GCTGGAATCCAAGATCCGTTCAC-3'	This study	N/A
Human *HMGCS1* primer forward: 5'-CTCCCTGACGTGGAATGTCT-3'	This study	N/A
Human *HMGCS1* primer reverse: 5'-GAACTGTCTGCCCAGGTGAT-3'	This study	N/A
Human *HMGCR* primer forward: 5'-GACGTGAACCTATGCTGGTCAG-3'	This study	N/A
Human *HMGCR* primer reverse: 5'-GGTATCTGTTTCAGCCACTAAGG-3'	This study	N/A

Human *MVK* primer forward: 5'-CACCTCAGAGCAAGTGGAGAAG-3'	This study	N/A
Human *MVK* primer reverse: 5'-TGCTGCCAGACACACCGAGTAG-3'	This study	N/A
Human *MVD* primer forward: 5'-CTCGGTGAAGTCCTTGCTGATG-3'	This study	N/A
Human *MVD* primer reverse: 5'-AGCGCGATGAAGAGCTGGTTC-3'	This study	N/A
Human *IDI1* primer forward: 5'-CTCCTGGCAGAGATGTGTATCC-3'	This study	N/A
Human *IDI1* primer reverse: 5'-CGGCTGGATTGCTTAATGGATG-3'	This study	N/A
Human *NSDHL* primer forward: 5'-GGATCGGTGGCTCTGGATTC-3'	This study	N/A
Human *NSDHL* primer reverse: 5'-GCAGAGGTCACCCAGAAAG-3'	This study	N/A
Human *SQLE* primer forward: 5'-CTCCAAGTTCAGGAAAAGCCTGC-3'	This study	N/A
Human *SQLE* primer reverse: 5'-GAGAACTGGACTCGGGTTAGCT-3'	This study	N/A
Human *CYP51A1* primer forward: 5'-CTCTTACCAGGTTGGCTGCCTT-3'	This study	N/A
Human *CYP51A1*primer reverse: 5'-CTTGAGACTGTCTGCGTTTCTGG-3'	This study	N/A
Human *DHCR7* primer forward: 5'-CAGCGCCAGAGACTGCAAA-3'	This study	N/A

Human *DHCR7* primer reverse: 5'-CAGCTTGAATCAAACCACTTCCC-3'	This study	N/A
Human *FDFT1* primer forward: 5'-TGTGACCTCTGAACAGGAGTGG-3'	This study	N/A
Human *FDFT1* primer reverse: 5'-CCCATAGAGTTGGCACGTTCTG-3'	This study	N/A
Human *LDLR* primer forward: 5'-CACGAAGTCAGGAAGATG-3'	This study	N/A
Human *LDLR* primer reverse: 5'-GGGTGCTGCAGATCATTC-3'	This study	N/A
Human *SREBF2* primer forward: 5'-GCTGCCAAGGAGAGTCTATAC-3'	This study	N/A
Human *SREBF2* primer reverse: 5'-GGCCTGAGGTTTCACCAAG-3'	This study	N/A
Human *SCAP* primer forward: 5'-CAAGAACCTCCTGGCAGTAG-3'	This study	N/A
Human *SCAP* primer reverse: 5'-CATGGAAGCGTTCCCAGTC-3'	This study	N/A
Human *INSIG1* primer forward: 5'-TAGCCCTGGTGCTCAAC-3'	This study	N/A
Human *INSIG1* primer reverse: 5'-AGCACTGGCGTGGTTAATG-3'	This study	N/A
Human *LGALS3* primer forward: 5'-GATGCGTTATCTGGGTCTGG-3'	This study	N/A
Human *LGALS3* primer reverse: 5'-GCACTTGGCTGTCCAGAAGATG-3'	This study	N/A

Human *ABCA1* primer forward: 5'-GATGCGTTATCTGGGTCTGG-3'	This study	N/A
Human *ABCA1* primer reverse: 5'-GCACTTGGCTGTCCAGAAGATG-3'	This study	N/A
Human *ACAT1* primer forward: 5'-CAGTAACAGCTGCCAATGC-3'	This study	N/A
Human *ACAT1* primer reverse: 5'-GGTTCTACAGCAGCGTCAG-3'	This study	N/A
Recombinant DNA		
SCAP shRNA#1	Horizon (Dharmacon)	Cat#V3SH11240_227412984
SCAP shRNA#2	Horizon (Dharmacon)	Cat#V3SH11240_228955440
SCAP shRNA#3	Horizon (Dharmacon)	Cat#V3SH11240_228534848
Insig1 shRNA#1	Horizon (Dharmacon)	Cat#V3SH11240_227321339
Insig1 shRNA#2	Horizon (Dharmacon)	Cat#V3SH11240_228332166
Insig1 shRNA#3	Horizon (Dharmacon)	Cat#V3SH11240_226630552
HMGCR shRNA#1	Horizon (Dharmacon)	Cat#V3SH11240_225596673

HMGCR shRNA#2	Horizon (Dharmacon)	Cat#V3SH11240_224997227
HMGCR shRNA#3	Horizon (Dharmacon)	Cat#V3SH11240_226661673
Non-targeting shRNA	Horizon (Dharmacon)	Cat#VSC11716
pcDNA-EF-Gal3_GFP	This study	
Software and algorithms		
ImageJ		https://imagej.net/ij/
GSEA		https://www.gsea-msigdb.org/gsea/index.jsp
Graphpad Prism	PRISM 10	licensed

482

483 **EXPERIMENTAL MODEL DETAILS**

484 **CELL CULTURE**

485 THP1 and THP1 dual monocytes purchased from ECACC were used in this study. Both THP1
486 and THP1 dual monocytes were cultured in RPMI 1640 containing 10% FBS and 1 mM sodium
487 pyruvate at 37^0C in a 5% CO_2 humidified incubator. They were differentiated into macrophages
488 using 100 nM Phorbol-13-myristate 13-acetate (PMA) for 24 hours, followed by media change.
489 Following a resting period of 48 hours, cells were utilized for respective experiments.

490 **BACTERIAL STRAINS AND MEDIA**

491 Mtb Erdmann strain was grown in Middlebrook 7H9 medium with 4% Albumin-dextrose-saline Or
492 Middlebrook 7H10 plates supplemented with 10% oleic acid-albumin-dextrose-catalase (OADC)
493 at 37^0C. A final concentration of 0.05% Tween 80 was added to the liquid medium.

494 **METHOD DETAILS**

495 **RNA sequencing and analysis:**

496 Total RNA was isolated from the Mtb-infected macrophages after treatment with anti-TB drugs
497 (Isoniazid and rifampicin) in the presence or absence of sertraline for 18 hours. Total RNA was
498 used for stranded library preparation and paired-end clustering with 150bp x 2 end of sequencing
499 performed on HiSeqX (Illumina) by Medgenome Labs. Raw and processed RNA-Seq data are
500 openly available on_____. Quality check of raw sequenced reads was performed using
501 Fastqc 0.12.1 and summarized with Multiqc 0.4. Adapters (Illumina universal adapters) and poor-
502 quality bases were trimmed using Trimmomatic 0.39. The trimmed reads were aligned to the
503 human genome gtf (v44) using Star (2.7.10b). Finally, the rawcounts matrix was generated using
504 Subread 2.0.6. Differential gene expression analysis was conducted via edgeR3.42.4. Gene set
505 enrichment analysis was used to compare datasets.

506 **Quantitative PCR:**

507 RNA was isolated using RNAzol (Sigma), and cDNA was synthesised using oligo-dT primers
508 using Verso cDNA synthesis kit following the manufacturer's protocol. Quantitative PCR was
509 performed using KAPA SYBR green (Sigma) on a LightCycler480 (Roche).

510 **Total cholesterol estimation:**

511 THP1 monocytes were seeded in 24-well plate at a density of 0.5*10^6 cells. Cells after washing
512 with 1X PBS were lysed in 100ul of 1% Triton X-100 for 20 mins on ice. Protein was estimated by
513 the BCA protein estimation kit following the protocol given. For total lipid isolation, 400µL of
514 chloroform: methanol (1:2) was added along with 100µL of 50 mM citric acid. The mix was
515 vortexed and spun down. After the addition of 100µL of autoclaved water, the mix was vortexed
516 and spun down, and finally, 100µL of chloroform was added. After centrifugation of the mix at

517 12000g for 10 minutes, the lower phase was collected and vacuum centrifuged for 30 minutes.
518 The pellet was diluted in cholesterol assay buffer, and total cholesterol levels were assessed
519 using the Total Cholesterol & Cholesteryl Ester Colorimetric Assay Kit (ab282928) following the
520 recommended protocol. Values were normalized with the protein content.

521 **Macrophage infection:**

522 The Mtb culture was centrifuged and washed with PBST (1x PBS with 0.05% of Tween 80) twice,
523 and single cell suspension was made after spinning down the culture at 800g for 10 minutes.
524 THP1 dual macrophages were infected for 6 hours at MOI5. After 6 hours, cells were washed
525 twice with 1X PBS, and appropriate cell culture media was added.

526 **Intracellular bacterial growth assay:**

527 THP1 dual monocytes were seeded in a 48-well plate at a density of 0.15 million cells. Cells were
528 differentiated into macrophages as indicated, and after a 48-hour of resting period, cells were
529 infected with Mtb for 6 hours at MOI5. After stopping the infection, cells were treated with drugs
530 isoniazid (20ng/mL), rifampicin (100ng/mL), and sertraline (20μM) given in 10% FBS RPMI media.
531 At day 3 post-treatment, cells were lysed with water containing 0.05% Tween 80, and dilutions of
532 intracellular bacteria were made in PBST. The final diluted lysate was plated on 7H10 plates.
533 To restrict cholesterol uptake by the macrophages, treatment with TB drugs was given in RPMI
534 media supplemented with 10% Lipoprotein-deficient serum (LPDS).
535 For the cholesterol replenishment assay, Mtb-infected THP1 macrophages were treated with
536 cholesterol (2μg/ml) for an hour after infection, followed by incubation with anti-TB drugs in LPDS
537 medium and further cholesterol was added every 24 hours.

538 **Immunoblotting**

539 THP1 dual macrophages were lysed in RIPA buffer along with a protease inhibitor cocktail.
540 Protein concentration was estimated by BCA assay, and 50μg of total protein was loaded per
541 sample in a 10% polyacrylamide gel. Protein was transferred to a nitrocellulose membrane, and
542 the membrane was blocked using a 5% BSA solution. The membrane was next incubated

543 overnight in anti-rabbit SREBP2 antibody, on shaking at 4°C. Next, the membrane was washed
544 thrice with PBST (1X PBS with 0.05% Tween 20) solution and incubated with HRP-conjugated
545 secondary antibody for an hour at room temperature. After washing with PBST, the membrane
546 was imaged using ImageQuant LAS 500.

547 **Filipin Staining:**

548 The THP1 macrophages were seeded in confocal chamber slides (1.5*10^4 cells per chamber)
549 and treated with sertraline at 20μM for 24 hours. Cells were washed twice with 1x PBS before
550 fixation with 4% methanol-free formaldehyde in 1X PHEM buffer for 20 mins at room temperature.
551 After an additional wash with 1x PBS, cells were stained with filipin staining solution (50ug/ml
552 diluted in 1x PBS) for an hour in the dark at room temperature. Next, the cells were washed with
553 1x PBS and imaged on a Leica SP8 laser scanning confocal microscope. Filipin was excited at
554 405nm laser.

555 **Cholesterol compartmentalization assay:**

556 THP1 monocytes were seeded at a density of 0.15 million cells in a four-chamber confocal dish
557 and differentiated as mentioned. The NBD-cholesterol at a final conc of 10μM was added for 24
558 hours along with the different compounds such as sertraline (20μM), citalopram (20μM), and
559 U18666A (2μg/ml). Before initiation of imaging, cells were stained with lysotracker Red (100nM)
560 along with Hoechst dye for 1 hour in 10% FBS containing RPMI. Images were taken using a Leica
561 SP8 laser scanning confocal microscope.

562 **Stable knockdown/overexpression cell line generation:**

563 Lenti-X 293T cells were transfected with pVSVG and pDR2.8 plasmids together with lentiviral
564 constructs expressing gene-specific shRNA or non-targeting controls to generate viral particles.
565 After 6 hours of transfection, the media was changed to 2% FBS containing DMEM, and after 48
566 hours, the cell supernatant was collected and centrifuged at 100g for 5 minutes to remove cell
567 debris. Further, this supernatant was filtered through a 0.45μ syringe filter, and viral particles were
568 concentrated using a 30kDa centricon filter. For transduction in THP1 monocytes, 50,000 cells

569 were seeded in a 24-well plate, and 100µL of viral stock was added along with a final
570 concentration of 8µg/mL polybrene. After 24 hours media was changed, and antibiotic selection
571 was initiated after 48 hours of transduction with 0.6µg/mL of puromycin. Cells showing tRFP
572 fluorescence co-expressed with shRNA were checked regularly.
573 The hGal3 and eGFP are excised from the pEGFP-hGal3 plasmid using Nhe1, Nde1 and Msc1
574 restriction enzymes and ligated to Xba1 and Msc1 digested pcDNA 3.1 vector. The final plasmid
575 is transfected in THP1 monocytes using Lipofectamine LTX.
576 **Galectin 3 puncta assessment:**
577 GFP tagged galectin-3 overexpressing THP1 monocytes were seeded in a chambered confocal
578 dish and treated with sertraline (20µM), citalopram (20µM), U18666A (2µg/ml) for 24 hours, and
579 with 1mM LLOMe for 15 minutes. Before imaging, cells were stained with Lyostracker Red and
580 Hoechst for an hour. Images were taken using a Leica SP8 laser scanning confocal microscope.
581 **Mitochondrial ROS estimation:**
582 THP1 dual cells were differentiated as indicated. Treatment was given with rotenone at 10µM for
583 30 minutes or with different indicated compounds. The cells were incubated with 5µM of MitoSox
584 dye for 30 minutes. After washing with 1X PBS, cells were imaged in the Invitrogen™ EVOS™
585 M5000 Imaging System.
586 **ELISA:**
587 THP1 dual macrophages were infected with Mtb at MOI5 and treated with different compounds.
588 Supernatant was collected at the indicated time points and filtered through a 0.2µ filter.
589 Concentration of IL-1β was determined using an ELISA kit following the recommended protocol.
590 **Statistical analysis**
591 The results are depicted as mean ± SEM. Statistical analysis was carried out using Student's t-
592 test (Welch's test or Mann-Whitney test) using GraphPad Prism. P values less than 0.05, 0.01,
593 0.005 are represented as *, ** and *** respectively.
594

595 **References:**

596 1. Chakaya, J., Petersen, E., Nantanda, R., Mungai, B.N., Migliori, G.B., Amanullah, F.,
597 Lungu, P., Ntoumi, F., Kumarasamy, N., Maeurer, M., and Zumla, A. (2022). The WHO
598 Global Tuberculosis 2021 Report - not so good news and turning the tide back to End
599 TB. Int J Infect Dis *124 Suppl 1*, S26-S29. 10.1016/j.ijid.2022.03.011.
600 2. Global tuberculosis report 2024. (2024).
601 3. Trajman, A., Campbell, J.R., Kunor, T., Ruslami, R., Amanullah, F., Behr, M.A., and
602 Menzies, D. (2025). Tuberculosis. Lancet *405*, 850-866. 10.1016/S0140-6736(24)02479-
603 6.
604 4. Tobin, E.H., and Tristram, D. (2025). Tuberculosis Overview. In StatPearls.
605 5. Matteelli, A., Lovatti, S., Rossi, B., and Rossi, L. (2025). Update on multidrug-resistant
606 tuberculosis preventive therapy toward the global tuberculosis elimination. Int J Infect
607 Dis *155*, 107849. 10.1016/j.ijid.2025.107849.
608 6. Nahid, P., Mase, S.R., Migliori, G.B., Sotgiu, G., Bothamley, G.H., Brozek, J.L.,
609 Cattamanchi, A., Cegielski, J.P., Chen, L., Daley, C.L., et al. (2019). Treatment of Drug-
610 Resistant Tuberculosis. An Official ATS/CDC/ERS/IDSA Clinical Practice Guideline. Am
611 J Respir Crit Care Med *200*, e93-e142. 10.1164/rccm.201909-1874ST.
612 7. Young, C., Walzl, G., and Du Plessis, N. (2020). Therapeutic host-directed strategies to
613 improve outcome in tuberculosis. Mucosal Immunol *13*, 190-204. 10.1038/s41385-019-
614 0226-5.
615 8. Wong, E.B., Cohen, K.A., and Bishai, W.R. (2013). Rising to the challenge: new
616 therapies for tuberculosis. Trends Microbiol *21*, 493-501. 10.1016/j.tim.2013.05.002.
617 9. Shankaran, D., Singh, A., Dawa, S., Arumugam, P., Gandotra, S., and Rao, V. (2023).
618 The antidepressant sertraline provides a novel host directed therapy module for
619 augmenting TB therapy. Elife *12*. 10.7554/eLife.64834.
620 10. Singh, A., Bisht, K., Yadav, N., Nanda, R., and Rao, V. (2025). Inflammasome activation
621 dictates the efficacy of antimycobacterial activity of frontline TB drugs. bioRxiv,
622 2025.2004.2002.646750. 10.1101/2025.04.02.646750.
623 11. King, R.J., Singh, P.K., and Mehla, K. (2022). The cholesterol pathway: impact on
624 immunity and cancer. Trends Immunol *43*, 78-92. 10.1016/j.it.2021.11.007.
625 12. Canfran-Duque, A., Rotllan, N., Zhang, X., Andres-Blasco, I., Thompson, B.M., Sun, J.,
626 Price, N.L., Fernandez-Fuertes, M., Fowler, J.W., Gomez-Coronado, D., et al. (2023).
627 Macrophage-Derived 25-Hydroxycholesterol Promotes Vascular Inflammation,
628 Atherogenesis, and Lesion Remodeling. Circulation *147*, 388-408.
629 10.1161/CIRCULATIONAHA.122.059062.
630 13. Reboldi, A., and Dang, E. (2018). Cholesterol metabolism in innate and adaptive
631 response. F1000Res *7*. 10.12688/f1000research.15500.1.
632 14. de Freitas, F.A., Levy, D., Reichert, C.O., Cunha-Neto, E., Kalil, J., and Bydlowski, S.P.
633 (2022). Effects of Oxysterols on Immune Cells and Related Diseases. Cells *11*.
634 10.3390/cells11081251.
635 15. Cyster, J.G., Dang, E.V., Reboldi, A., and Yi, T. (2014). 25-Hydroxycholesterols in innate
636 and adaptive immunity. Nat Rev Immunol *14*, 731-743. 10.1038/nri3755.
637 16. Duewell, P., Kono, H., Rayner, K.J., Sirois, C.M., Vladimer, G., Bauernfeind, F.G., Abela,
638 G.S., Franchi, L., Nunez, G., Schnurr, M., et al. (2010). NLRP3 inflammasomes are
639 required for atherogenesis and activated by cholesterol crystals. Nature *464*, 1357-1361.
640 10.1038/nature08938.
641 17. Parihar, S.P., Guler, R., Khutlang, R., Lang, D.M., Hurdayal, R., Mhlanga, M.M., Suzuki,
642 H., Marais, A.D., and Brombacher, F. (2014). Statin therapy reduces the mycobacterium
643 tuberculosis burden in human macrophages and in mice by enhancing autophagy and
644 phagosome maturation. J Infect Dis *209*, 754-763. 10.1093/infdis/jit550.

645 18. Schonewille, M., de Boer, J.F., Mele, L., Wolters, H., Bloks, V.W., Wolters, J.C.,
646 Kuivenhoven, J.A., Tietge, U.J., Brufau, G., and Groen, A.K. (2016). Statins increase
647 hepatic cholesterol synthesis and stimulate fecal cholesterol elimination in mice. J Lipid
648 Res *57*, 1455-1464. 10.1194/jlr.M067488.
649 19. Wong, J., Quinn, C.M., Gelissen, I.C., Jessup, W., and Brown, A.J. (2008). The effect of
650 statins on ABCA1 and ABCG1 expression in human macrophages is influenced by
651 cellular cholesterol levels and extent of differentiation. Atherosclerosis *196*, 180-189.
652 10.1016/j.atherosclerosis.2007.03.030.
653 20. Chen, L., Zhang, J., Xu, W., Chen, J., Tang, Y., Xiong, S., Li, Y., Zhang, H., Li, M., and
654 Liu, Z. (2024). Cholesterol-rich lysosomes induced by respiratory syncytial virus promote
655 viral replication by blocking autophagy flux. Nat Commun *15*, 6311. 10.1038/s41467-
656 024-50711-4.
657 21. Eid, W., Dauner, K., Courtney, K.C., Gagnon, A., Parks, R.J., Sorisky, A., and Zha, X.
658 (2017). mTORC1 activates SREBP-2 by suppressing cholesterol trafficking to lysosomes
659 in mammalian cells. Proc Natl Acad Sci U S A *114*, 7999-8004.
660 10.1073/pnas.1705304114.
661 22. Radhakrishnan, A., Ikeda, Y., Kwon, H.J., Brown, M.S., and Goldstein, J.L. (2007).
662 Sterol-regulated transport of SREBPs from endoplasmic reticulum to Golgi: oxysterols
663 block transport by binding to Insig. Proc Natl Acad Sci U S A *104*, 6511-6518.
664 10.1073/pnas.0700899104.
665 23. Frolov, A., Zielinski, S.E., Crowley, J.R., Dudley-Rucker, N., Schaffer, J.E., and Ory,
666 D.S. (2003). NPC1 and NPC2 regulate cellular cholesterol homeostasis through
667 generation of low density lipoprotein cholesterol-derived oxysterols. J Biol Chem *278*,
668 25517-25525. 10.1074/jbc.M302588200.
669 24. Peake, K.B., and Vance, J.E. (2010). Defective cholesterol trafficking in Niemann-Pick
670 C-deficient cells. FEBS Lett *584*, 2731-2739. 10.1016/j.febslet.2010.04.047.
671 25. DeBose-Boyd, R.A., Brown, M.S., Li, W.P., Nohturfft, A., Goldstein, J.L., and
672 Espenshade, P.J. (1999). Transport-dependent proteolysis of SREBP: relocation of site-
673 1 protease from Golgi to ER obviates the need for SREBP transport to Golgi. Cell *99*,
674 703-712. 10.1016/s0092-8674(00)81668-2.
675 26. Hu, P., Li, H., Sun, W., Wang, H., Yu, X., Qing, Y., Wang, Z., Zhu, M., Xu, J., Guo, Q.,
676 and Hui, H. (2021). Cholesterol-associated lysosomal disorder triggers cell death of
677 hematological malignancy: Dynamic analysis on cytotoxic effects of LW-218. Acta
678 Pharm Sin B *11*, 3178-3192. 10.1016/j.apsb.2021.02.004.
679 27. Alvarez-Valadez, K., Sauvat, A., Diharce, J., Leduc, M., Stoll, G., Guittat, L.,
680 Lambertucci, F., Paillet, J., Motino, O., Ferret, L., et al. (2025). Lysosomal damage due
681 to cholesterol accumulation triggers immunogenic cell death. Autophagy *21*, 934-956.
682 10.1080/15548627.2024.2440842.
683 28. Aits, S., Kricker, J., Liu, B., Ellegaard, A.M., Hamalisto, S., Tvingsholm, S., Corcelle-
684 Termeau, E., Hogh, S., Farkas, T., Holm Jonassen, A., et al. (2015). Sensitive detection
685 of lysosomal membrane permeabilization by lysosomal galectin puncta assay.
686 Autophagy *11*, 1408-1424. 10.1080/15548627.2015.1063871.
687 29. Thiele, D.L., and Lipsky, P.E. (1990). The action of leucyl-leucine methyl ester on
688 cytotoxic lymphocytes requires uptake by a novel dipeptide-specific facilitated transport
689 system and dipeptidyl peptidase I-mediated conversion to membranolytic products. J
690 Exp Med *172*, 183-194. 10.1084/jem.172.1.183.
691 30. Davis, O.B., Shin, H.R., Lim, C.Y., Wu, E.Y., Kukurugya, M., Maher, C.F., Perera, R.M.,
692 Ordonez, M.P., and Zoncu, R. (2021). NPC1-mTORC1 Signaling Couples Cholesterol
693 Sensing to Organelle Homeostasis and Is a Targetable Pathway in Niemann-Pick Type
694 C. Dev Cell *56*, 260-276 e267. 10.1016/j.devcel.2020.11.016.

31. Martin, L.A., Kennedy, B.E., and Karten, B. (2016). Mitochondrial cholesterol: mechanisms of import and effects on mitochondrial function. J Bioenerg Biomembr *48*, 137-151. 10.1007/s10863-014-9592-6.
32. de la Mata, M., Cotan, D., Villanueva-Paz, M., de Lavera, I., Alvarez-Cordoba, M., Luzon-Hidalgo, R., Suarez-Rivero, J.M., Tiscornia, G., and Oropesa-Avila, M. (2016). Mitochondrial Dysfunction in Lysosomal Storage Disorders. Diseases *4*. 10.3390/diseases4040031.
33. Goicoechea, L., Conde de la Rosa, L., Torres, S., Garcia-Ruiz, C., and Fernandez-Checa, J.C. (2023). Mitochondrial cholesterol: Metabolism and impact on redox biology and disease. Redox Biol *61*, 102643. 10.1016/j.redox.2023.102643.
34. Balboa, E., Castro, J., Pinochet, M.J., Cancino, G.I., Matias, N., Saez, P.J., Martinez, A., Alvarez, A.R., Garcia-Ruiz, C., Fernandez-Checa, J.C., and Zanlungo, S. (2017). MLN64 induces mitochondrial dysfunction associated with increased mitochondrial cholesterol content. Redox Biol *12*, 274-284. 10.1016/j.redox.2017.02.024.
35. Lin, J.X., Xu, C.Y., Wu, X.M., Che, L., Li, T.Y., Mo, S.M., Guo, D.B., Lin, Z.N., and Lin, Y.C. (2023). Rab7a-mTORC1 signaling-mediated cholesterol trafficking from the lysosome to mitochondria ameliorates hepatic lipotoxicity induced by aflatoxin B1 exposure. Chemosphere *320*, 138071. 10.1016/j.chemosphere.2023.138071.
36. Mari, M., Morales, A., Colell, A., Garcia-Ruiz, C., and Fernandez-Checa, J.C. (2009). Mitochondrial glutathione, a key survival antioxidant. Antioxid Redox Signal *11*, 2685-2700. 10.1089/ARS.2009.2695.
37. Guo, C., Chi, Z., Jiang, D., Xu, T., Yu, W., Wang, Z., Chen, S., Zhang, L., Liu, Q., Guo, X., et al. (2018). Cholesterol Homeostatic Regulator SCAP-SREBP2 Integrates NLRP3 Inflammasome Activation and Cholesterol Biosynthetic Signaling in Macrophages. Immunity *49*, 842-856 e847. 10.1016/j.immuni.2018.08.021.
38. Hu, T., Liu, C.H., Lei, M., Zeng, Q., Li, L., Tang, H., and Zhang, N. (2024). Metabolic regulation of the immune system in health and diseases: mechanisms and interventions. Signal Transduct Target Ther *9*, 268. 10.1038/s41392-024-01954-6.
39. Andersson, M., Aronsen, K.F., Balch, C., Domellof, L., Eksborg, S., Hafstrom, L.O., Howell, S.B., Karesen, R., Midander, J., and Teder, H. (1989). Pharmacokinetics of intra-arterial mitomycin C with or without degradable starch microspheres (DSM) in the treatment of non-resectable liver cancer. Acta Oncol *28*, 219-222. 10.3109/02841868909111250.
40. Omotade, T.O., and Roy, C.R. (2019). Manipulation of Host Cell Organelles by Intracellular Pathogens. Microbiol Spectr *7*. 10.1128/microbiolspec.BAI-0022-2019.
41. Clemente, T.M., Angara, R.K., and Gilk, S.D. (2023). Establishing the intracellular niche of obligate intracellular vacuolar pathogens. Front Cell Infect Microbiol *13*, 1206037. 10.3389/fcimb.2023.1206037.
42. Perez-Guzman, C., and Vargas, M.H. (2006). Hypocholesterolemia: a major risk factor for developing pulmonary tuberculosis? Med Hypotheses *66*, 1227-1230. 10.1016/j.mehy.2005.12.041.
43. Jo, Y.S., Han, K., Kim, D., Yoo, J.E., Kim, Y., Yang, B., Choi, H., Sohn, J.W., Shin, D.W., and Lee, H. (2021). Relationship between total cholesterol level and tuberculosis risk in a nationwide longitudinal cohort. Sci Rep *11*, 16254. 10.1038/s41598-021-95704-1.
44. Chidambaram, V., Zhou, L., Ruelas Castillo, J., Kumar, A., Ayeh, S.K., Gupte, A., Wang, J.Y., and Karakousis, P.C. (2021). Higher Serum Cholesterol Levels Are Associated With Reduced Systemic Inflammation and Mortality During Tuberculosis Treatment Independent of Body Mass Index. Front Cardiovasc Med *8*, 696517. 10.3389/fcvm.2021.696517.

45. Parivakkam Mani, A., K, S., K, D.K., and Yadav, S. (2023). Assessment of Lipid Profile in Patients With Pulmonary Tuberculosis: An Observational Study. Cureus *15*, e39244. 10.7759/cureus.39244.
46. Bah, S.Y., Dickinson, P., Forster, T., Kampmann, B., and Ghazal, P. (2017). Immune oxysterols: Role in mycobacterial infection and inflammation. J Steroid Biochem Mol Biol *169*, 152-163. 10.1016/j.jsbmb.2016.04.015.
47. Hayakawa, S., Tamura, A., Nikiforov, N., Koike, H., Kudo, F., Cheng, Y., Miyazaki, T., Kubekina, M., Kirichenko, T.V., Orekhov, A.N., et al. (2022). Activated cholesterol metabolism is integral for innate macrophage responses by amplifying Myd88 signaling. JCI Insight *7*. 10.1172/jci.insight.138539.
48. Istvan, E.S., and Deisenhofer, J. (2001). Structural mechanism for statin inhibition of HMG-CoA reductase. Science *292*, 1160-1164. 10.1126/science.1059344.
49. Xu, J.F., Washko, G.R., Nakahira, K., Hatabu, H., Patel, A.S., Fernandez, I.E., Nishino, M., Okajima, Y., Yamashiro, T., Ross, J.C., et al. (2012). Statins and pulmonary fibrosis: the potential role of NLRP3 inflammasome activation. Am J Respir Crit Care Med *185*, 547-556. 10.1164/rccm.201108-1574OC.
50. Henriksbo, B.D., Lau, T.C., Cavallari, J.F., Denou, E., Chi, W., Lally, J.S., Crane, J.D., Duggan, B.M., Foley, K.P., Fullerton, M.D., et al. (2014). Fluvastatin causes NLRP3 inflammasome-mediated adipose insulin resistance. Diabetes *63*, 3742-3747. 10.2337/db13-1398.
51. Altaf, A., Qu, P., Zhao, Y., Wang, H., Lou, D., and Niu, N. (2015). NLRP3 inflammasome in peripheral blood monocytes of acute coronary syndrome patients and its relationship with statins. Coron Artery Dis *26*, 409-421. 10.1097/MCA.0000000000000255.
52. Ebrahimi-Fakhari, D., Wahlster, L., Bartz, F., Werenbeck-Ueding, J., Praggastis, M., Zhang, J., Joggerst-Thomalla, B., Theiss, S., Grimm, D., Ory, D.S., and Runz, H. (2016). Reduction of TMEM97 increases NPC1 protein levels and restores cholesterol trafficking in Niemann-pick type C1 disease cells. Hum Mol Genet *25*, 3588-3599. 10.1093/hmg/ddw204.
53. Nishimura, T., Inoue, T., Shibata, N., Sekine, A., Takabe, W., Noguchi, N., and Arai, H. (2005). Inhibition of cholesterol biosynthesis by 25-hydroxycholesterol is independent of OSBP. Genes Cells *10*, 793-801. 10.1111/j.1365-2443.2005.00879.x.
54. Choi, H., Kim, H.J., Lee, S.E., Song, H.H., Kim, J., Han, J., Jeong, J.H., Lee, D.Y., Chang, S., and Mook-Jung, I. (2025). 25-Hydroxycholesterol modulates microglial function and exacerbates Alzheimer's disease pathology: mechanistic insights and therapeutic potential of cholesterol esterification inhibition. J Neuroinflammation *22*, 50. 10.1186/s12974-025-03357-y.
55. Griffiths, W.J., and Wang, Y. (2022). Cholesterol metabolism: from lipidomics to immunology. J Lipid Res *63*, 100165. 10.1016/j.jlr.2021.100165.
56. Reboldi, A., Dang, E.V., McDonald, J.G., Liang, G., Russell, D.W., and Cyster, J.G. (2014). Inflammation. 25-Hydroxycholesterol suppresses interleukin-1-driven inflammation downstream of type I interferon. Science *345*, 679-684. 10.1126/science.1254790.
57. Viaud, M., Ivanov, S., Vujic, N., Duta-Mare, M., Aira, L.E., Barouillet, T., Garcia, E., Orange, F., Dugail, I., Hainault, I., et al. (2018). Lysosomal Cholesterol Hydrolysis Couples Efferocytosis to Anti-Inflammatory Oxysterol Production. Circ Res *122*, 1369-1384. 10.1161/CIRCRESAHA.117.312333.
58. Zhou, R., Yazdi, A.S., Menu, P., and Tschopp, J. (2011). A role for mitochondria in NLRP3 inflammasome activation. Nature *469*, 221-225. 10.1038/nature09663.
59. Leishman, S., Aljadeed, N.M., Qian, L., Cockcroft, S., Behmoaras, J., and Anand, P.K. (2024). Fatty acid synthesis promotes inflammasome activation through NLRP3 palmitoylation. Cell Rep *43*, 114516. 10.1016/j.celrep.2024.114516.

795 60. Kuzu, O.F., Toprak, M., Noory, M.A., and Robertson, G.P. (2017). Effect of
796 lysosomotropic molecules on cellular homeostasis. Pharmacol Res *117*, 177-184.
797 10.1016/j.phrs.2016.12.021.
798